Available online at www.sciencedirect.com
SCIENCE DIRECT
Polymer 46 (2005) 2163–2174
polymer
www.elsevier.com/locate/polymer

Organic–inorganic hybrid materials from a new octa(2,3-epoxypropyl)silsesquioxane with diamines

Long-Hua Lee[a,b], Wen-Chang Chen[a,b,*]

[a]Department of Chemical Engineering, National Taiwan University, No. 1, Sec.4, Roosevelt Road, Taipei 106, Taiwan, ROC
[b]Institute of Polymer Science and Engineering, National Taiwan University, No. 1, Sec.4, Roosevelt Road, Taipei 106, Taiwan, ROC

Received 2 October 2004; received in revised form 18 January 2005; accepted 20 January 2005

Abstract

Hybrid materials based on a new polyhedral oligomeric silsesquioxane, octa(2,3-epoxypropyl)silsesquioxane (**OE**) with diamines of 4,4′-methylenedianiline (DDM) and 5-trifluoromethyl-1,3-phenylenediamine (FPA) were prepared and characterized. **OE** was synthesized from cage-structured octaallylsilsesquioxane (**OA**) with *m*-chloroperbenzoicacid. The FTIR studies suggested that the N–H bond in diamines was not completely reacted with epoxy group due to steric hindrance and also extensive hydrogen bonding existed in the hybrid materials. The retention of the cage structure in the prepared hybrid materials was suggested by the FTIR and ^{29}Si NMR studies. The **OE/FPA** hybrid materials had superior thermal/mechanical characteristics than the **OE/DDM** due to the higher rigidity of the FPA than that of DDM or the silicon-fluorine interaction enhancing crosslinking reaction or hydrogen bonding. The prepared **OE/FPA** had a T_g of 170 °C, which was higher than diglycidyl ether of bisphenyl A (DGEBA)/DDM at the same stoichiometric ratio. It also had excellent thermal, mechanical, and dielectric characteristics with high storage modulus of 1.8 GPa (30 °C) and 0.3 GPa (250 °C), low coefficient of thermal expansion of 86 μm/m °C, and dielectric constant of 2.19. Thus, it can be high performance materials with potential applications for electronic packaging.

Keywords: Hybrid materials; Silsesquioxane; Epoxy

1. Introduction

Organic–inorganic hybrid materials have been recognized as a new class of advanced materials because of the versatile synthetic approaches and molecular tailing properties. Polyhedral oligomeric silsesquioxane (POSS) based nanocomposites are one of the widely studied hybrid materials [1]. The general formula of POSS is $[RSiO_{3/2}]_n$ consisted of a central core around 1 nm with different number of organic groups (R) on the corner. The feasibility of controlling the arm number, arm length, and arm functionality makes POSS topologically ideal for the preparation of nanocomposites.

The R group on the corner of POSS could be either inert or reactive functional group. For the former case, hydrogen, alkyl chain or phenyl chain is usually employed. For example, hydridosilsesquioxane (HSSQ) and methylsilsesquioxane (MSSQ) have been recognized as two important low dielectric constant materials for deep submicron integrated circuit process [2–6]. For the latter case, the POSS functionality employed for preparing the hybrid materials include acrylic [7], epoxy [8–13], amine [14,15], vinyl [16], hydrido [16], isocyanate [17], halide [18,19], and norbonyl [20]. Judicious organic–inorganic hybrid materials can be prepared by reacting the organic functional group (R) on the corner with desired monomer. The POSS used as the pendent group or the nano-crosslinker in the polymer matrix is obtained by the single or multifunctional functional group, respectively.

Epoxy polymers are one of the mostly widely studied engineering thermosets because of their excellent thermal, mechanical, and electrical properties. By incorporating POSS with the epoxy functionality offers the opportunity of enhancing physical properties for advanced electronic, aerospace and automotive applications. Incorporation of

* Corresponding author. Address: Department of Chemical Engineering, National Taiwan University, No. 1, Sec.4, Roosevelt Road, Taipei 106, Taiwan, ROC. Tel.: +886 2 23628398; fax: +886 2 23623040.
E-mail address: chenwc@ntu.edu.tw (W.-C. Chen).

0032-3861/$ - see front matter © 2005 Elsevier Ltd. All rights reserved.
doi:10.1016/j.polymer.2005.01.035

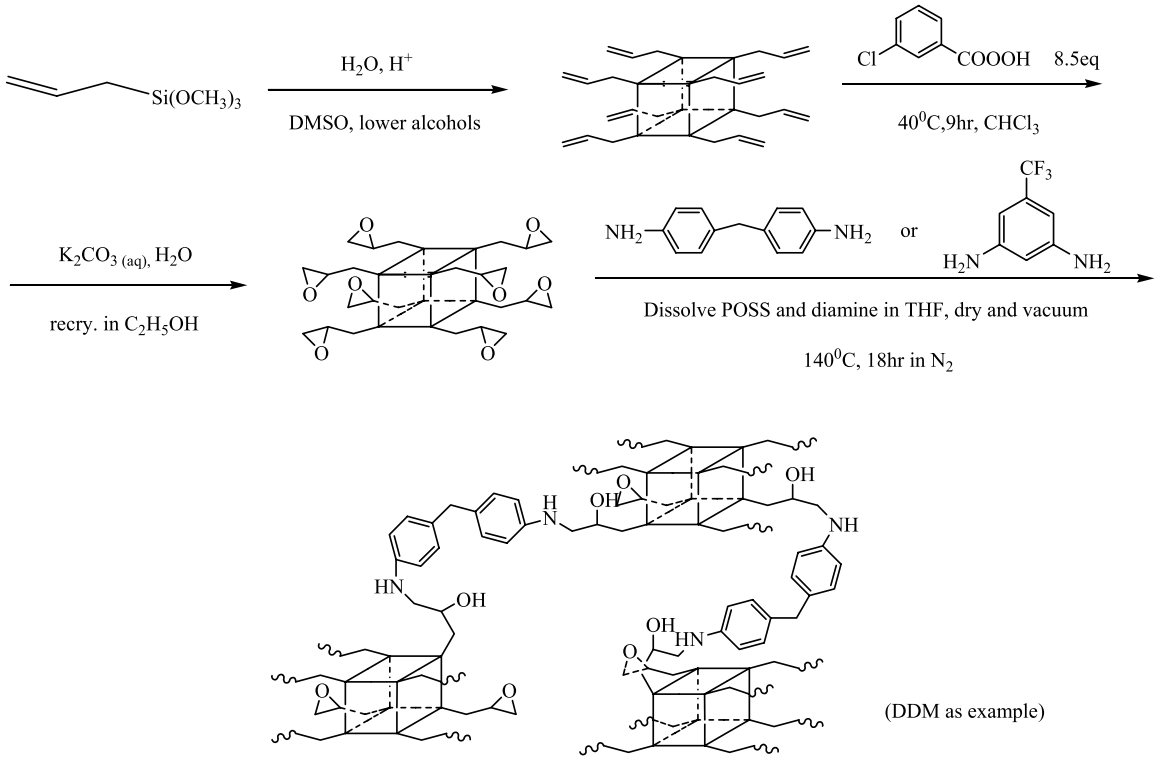

Scheme 1.

epoxy-monofunctionalized POSS in diamine-catalyzed resin results in retardation of network motion and enhanced T_g without increasing crosslinking density [10]. However, the presence of inert aliphatic groups, e.g. isobutyl, cyclopentyl, cyclohexyl, et al., results in phase separation due to incompatibility between such groups and epoxy/amine system [12]. Laine et al. reported new hybrid materials of octa(glycidylpropyldimethylsiloxy)silsesquioxane(OG)/DDM and octa(ethylcyclohexylepoxide) dimethylsiloxysilsesquioxane(OC)/DDM hybrids [9], which had high crosslinking density, mechanically rigidity and thermally degradation stability. However, the two hybrids materials exhibited much a lower T_g in comparison with conventional diglycidyl ether of bisphenyl A (DGEBA)/DDM system. Similar conclusion has also obtained from the system of OG/4,4′-diaminodiphenyl sulfone(DDS) [11]. The soft linkage of dimethylsiloxane and hydrocarbon chain between epoxy and POSS was suggested to explain the above result [11].

The tether rigidity on POSS may be enhanced by reducing chain length or increasing rigidity of the tether, which then effectively limits relaxation and enhances T_g of hybrid materials. One possible candidate is to use epoxidation of octavinylsilsesquioxane but with the difficulties of separating the product and complete epoxidation [21]. Martinova et al. [22] reported the successful synthesis of octaallylsilsesquioxane (**OA**) by hydrolysis and condensation of allyltrichlorosilane at −40 °C followed by purification under strict conditions. In this study, we explore another simple approach of synthesizing **OA** using allyltrimethoxysilane, as shown in Scheme 1. In the following, a new fully-epoxidized silsesquioxane, octa(2,3-epoxypropyl)silsesquioxane (**OE**), was synthesized using **OA** reacted with *m*-chloroperbenzoic acid (mCPBA). The **OE** was further reacted with two diamines, DDM and 5-trifluoromethyl-1,3-phenylenediamine (FPA), to form hybrid materials for characterization. The chemical structure, thermal, mechanical, and dielectric properties were analyzed and compared with previous reports in the literature [8–11].

2. Experimental section

2.1. Materials

Allyltrimethoxysilane (ATMS) was purchased from Gelest and used without further purification. Nitric acid and dimethyl sulfoxide (DMSO) was obtained from Wako and Tedia, respectively. *m*-Chloroperbenzoic acid (mCPBA, 70–75%, ACROS), potassium carbonate (anhydrous, p.a., ACROS), tetrahydrofuran (99.9%, ACROS), 4,4′-diaminodiphenylmethane (DDM, 97%, ACROS), and 5-trifluoromethyl-1,3-phenylenediamine (FPA, 97%, Lancaster) were used as received. $CDCl_3$ (99.8%, CIL) was used as NMR solvent.

2.2. Synthesis of Octaallylsilsesquioxane (**OA**)

Into a 100 ml three-necked round bottom flask were added 10.29 g H_2O (0.571 mmol), 0.8 g concentrated HNO_3, and 2.93 g DMSO (0.038 mmol). 30.94 g ATMS (0.181 mol) and another 5.87 g (0.075 mol) DMSO were mixed and placed in an addition funnel and added dropwise into the flask in 3 h at 60 °C. Upon completion of addition, the mixture was allowed to react for 6 h and then cool to room temperature, kept in dark at ambient for crystallization around 10 days. Layer separation occurred and cube/rod-shaped crystalline product was observed at bottom layer. The crystals were filtered, washed with methanol and vacuum dried. 311 mg product was obtained (yield: 1.75%). Although the yield of present synthesis is only 1.75%, the crystalline product is essentially pure and does not require sophisticated purification process. We believe that the yield could be improved if a suitable recrystallization solvent is found for **OA**. Another possible methodology is to prepare **OA** from the dehydrogenation of octapropyl silsesquioxane (**OP**) $[(SiO_{1.5})CH_2CH_2CH_3]_8$, using dehydrogenation. The solubility of **OP** in common organic solvent is much lower than **OA**, and thus high yield of crystalline **OP** could be obtained. Therefore, high yield of **OA** could be synthesized from **OP** by dehydrogenation. IR peak (cm^{-1}): 3083, 3065 (C=C–H), 3005, 2980, 2926, 2890 (C–C–H), 1636 (C=C), 1105 (Si–O–Si). NMR (δ, ppm, in $CDCl_3$): ^{1}H: 5.75 (1H, ddd, $J_{HH}=24.94$, 9.9, 7.8 Hz), 4.97 (1H, dd, $J_{HH}=17.15$, 1.4 Hz), 4.94 (1H, dd, $J_{HH}=10.35$, 1.4 Hz); and 1.62 (2H, d, $J=7.75$ Hz). ^{13}C(δ, ppm, in $CDCl_3$): 131.77 ($H_2C=\mathit{C}HCH_2Si$), 115.23 ($H_2\mathit{C}=CHCH_2Si$), and 19.21 ppm ($H_2C=CH\mathit{C}H_2Si$). ^{29}Si: −70.77 ppm. Elemental Analysis: Calcd: C: 38.66%, H: 5.37%, Anal.: C: 38.14%, H: 4.82%.

2.3. Synthesis of octa(2,3-epoxypropyl)silsesquioxane (**OE**)

Complete epoxidation and purification of **OA** was achieved using the following scheme: into a sample vial were added 0.15 g **OA** (0.2 mmol), 0.42 g mCPBA (1.71 mmol) and 10 ml chloroform. The system was purged with N_2, sealed and heated at 40 °C for 9 h. After cooling to room temperature, $K_2CO_{3(aq)}$ was added, the mixture was rigorously stirred and the water layer discarded. Deionized water and anhydrous $MgSO_4$ were then added. The organic layer was dried and the crude product was purified by recrystallization with ethanol. Yield: 75% (0.132 g). IR peak (cm^{-1}): 3052, 2994, 2924(C–H), 1107 (Si–O–Si), 837 (epoxy). NMR (δ, ppm, in $CDCl_3$): ^{1}H: 3.05 (1H, H_aH_b-C(O)CHCH$_2$Si), 2.79 (1H, H_aH_bC(O)CHCH$_2$Si), 2.46 (1H, H_2C(O)CHCH$_2$Si), 1.27 (1H, H_2C(O)CHCH_cH_dSi), and 0.92 (1H, H_2C(O)CHCH_cH_dSi); ^{13}C(δ, ppm, in $CDCl_3$): 48.3, 48.2, and 16.7 ppm; ^{29}Si: −69.7 ppm. Elemental Analysis: Calcd C: 32.99%, H: 4.58%, Anal.: C: 32.98%, H: 4.64%.

2.4. Preparation of **OE-DDM** hybrid nanocomposites

The quantity of DDM used in preparing **OE-DDM** hybrids was determined based on conventional concept that one N–H bond reacts exactly with one epoxide. When the stoichiometric ratio of amine groups and epoxides equals, the quantity of DDM is denoted as 100. Thus, the abbreviation of **OE-DDM-200** would indicate that the hybrid material consists of **OE** and DDM in which twice the stoichiometric amount of DDM was used. Take **OE-DDM-50** as an example: 0.12 g **OE** (0.13 mmol) and 0.056 g DDM (0.27 mmol) was dissolved and mixed in 0.76 g THF and the solution was transferred to Teflon watch glass and then dried in vacuum oven. The solids were cured in N_2 oven at 140 °C for 18 h and cooled to room temperature; yellowish, transparent and tough material was obtained.

2.5. Preparation of OE-FPA-200 hybrid nanocomposite

Preparation of **OE-FPA** was similar to that of **OE-DDM** as described above except FPA was used as curing agent. The **OE-FPA-200** was prepared to investigate the thermal, mechanical, and electronic properties of **OE**/fluoro-diamine nanocomposites.

2.6. Characterization

FTIR spectra were recorded using KBr windows on DigiLab FTS (Model: 3500GX). The residual epoxy in the prepared hybrid materials after curing was estimated as below: The ratio of the peak areas at 1107 cm^{-1} (Si–O–Si) to that at 837 cm^{-1} (epoxy) of the uncured **OE** was used as the reference. Then, the residual epoxy group in the hybrid materials was estimated by comparing the ratio of the peak area of 837 cm^{-1} to that at 1107 cm^{-1} with that of the uncured **OE**, which has eight epoxy groups. Liquid state ^{1}H and ^{13}C NMR spectra were obtained using a Bruker Avance 500 NMR, and ^{29}Si NMR spectrum on a JNX-EX 400 NMR. Solid state CP/MAS NMR of **OE-DDM-100–300** hybrids were conducted on Varian 400 MHz, while **OE-FPA-200** (^{19}F and ^{29}Si) on Varian Unity-Inova 500. MS analysis was obtained on Finnigan Mat 95S using Fast atom bombardment (FAB) method. Elemental analysis was conducted on HERAEUS VarioEL-β. Single crystal and powder X-ray diffraction analysis was made on Nonius CAD4 Kappa Axis XRD.

TGA and DSC thermal analysis were conducted on Dupont Model 951 thermogravimetric analyzer and Dupont Model 910S differential scanning calorimeter, respectively. The thermal-mechanical properties of the prepared materials were tested by a TA 2940 thermo mechanical analysis (TMA) and Perkin Elmer Instruments, DMA7e. The heating rate was 5 °C/min and the temperature operated from room temperature to 200 and 250 °C for TMA and DMA, respectively. Dielectric constant was determined at

30 °C and 100 kHz, using a TA instrument, DEA 2970 Dielectric Analyzer.

3. Results and discussions

3.1. Synthesis and characterization of *OA* and *OE*

Fig. 1 shows the FTIR spectra of **OA** and **OE**. The FTIR spectrum of **OA** shows a medium peak at 1635 cm^{-1} and a very strong peak at 1110 cm^{-1}, which are characteristics of C=C bond and cage-structured Si–O–Si stretching, respectively. However, the C=C stretching at 1635 cm^{-1} is completely disappeared and a characteristic epoxy peak at 837 cm^{-1} is shown in the spectrum of **OE**. It suggests the complete epoxidation of **OA**. Besides, the characteristic cage Si–O–Si peak at 1110 cm^{-1} exhibits a similar intensity and position in the spectra for both compounds, which suggests the cage structure remains intact during epoxidation.

Fig. 2(a) and (b) shows the ^{1}H and ^{13}C NMR spectra of **OA** and **OE**. The alkenic hydrogens in **OA** show distinct splitting patterns and the peak positions are in accordance with purely organic molecules bearing terminal alkenes. Complete epoxidation of **OA** to the corresponding **OE** was further evidenced in ^{1}H NMR as the alkenic proton peaks (5.75, 4.97 and 4.94 ppm) are completely replaced by upper field ones (3.05, 2.79, 2.46, 1.27 and 0.92 ppm). The presence of five distinct peaks at the ^{1}H NMR spectrum of **OE**, instead of four, is probably attributed to a unique environment of the two protons on the methylene bridge. Being sandwiched between the bulky silsesquioxane cage and the epoxy ring, the two protons lying on the different sides of carbon chain are influenced to different degrees. This is further confirmed in the coupling constant; constant as high as 14.95 Hz is an indication that the two protons can influence each other to such a great extent. The successful preparation of **OA** and **OE** is further confirmed by the ^{13}C and ^{29}Si NMR spectra, where the assignment of the peak positions is consistent with the proposed chemical structure. Note that ^{29}Si NMR spectrum of **OE** is available at Fig. 7(a), as discussed later.

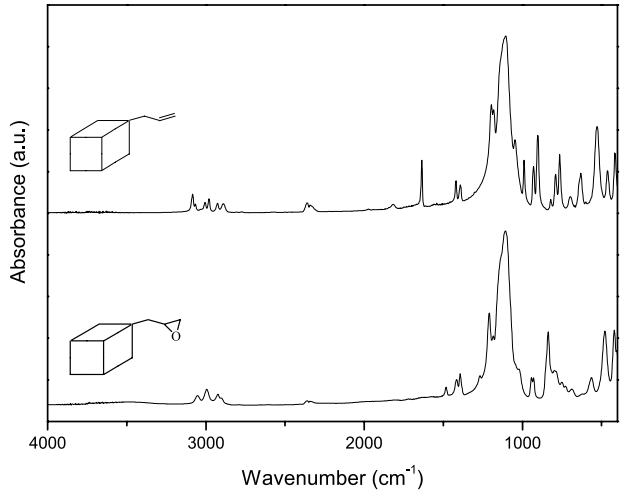

Fig. 1. FTIR absorption spectra of **OA** and **OE**.

Table 1
Crystallographic data for **OA**

Empirical formula	$C_{24}H_{40}O_{12}Si_8$
M_r	745.28
T/*K*	295(2)
Crystal system	Triclinic
Space group	P-1
a/Å	8.8530(2)
b/Å	10.2120(2)
c/Å	10.5490(2)
α/°	93.6560(10)
β/°	91.1740(10)
γ/°	94.4720(10)
V/Å^3	948.55(3)
Z	1
μ/mm^{-1}	0.334
Reflection collected	7322
Independent reflections (R_{int})	4324 (0.0196)
Goodness of fit on F^2	1.078
Final *R* indices	$R1=0.0622$, $wR2=0.1727$
R indices (all data)	$R1=0.0832$, $wR2=0.2005$
Largest diff. Peak and hole/e Å^{-3}	0.693 and −0.666
Bond length of Si–C/Å	1.838–1.842
Bond length of Si–O/Å	1.607–1.618
Bond length of C=C/Å	1.068–1.186
Bond length of C–C/Å	1.468–1.487
Bond angle of Si–O–Si/°	145.0–152.7
Bond angle of Si–C–C/°	112.8–115.1
Bond angle of O–Si–C/°	108.8–110.6
Bond angle of O–Si–O/°	108.8–110.6
Bond angle of C–C=C/°	133.4–147.1

Mass spectrum illustrates a parent peak at *m*/*z* equals to 745.0 and a base peak at 636.9 for **OA**. The weak intensity (6%) of the parent peak with respect to the base peak shows the labile nature of the allyl moiety. The two peaks at 702.9 and 660.9 are assigned to the molecular fragments without one and two allyl groups, respectively. It supports the conventional concept that allyl radicals/cations are relatively stable due to resonance and therefore readily ionized. The results are almost the same as those reported by Martynova et al. [22]. Peak of expected *m*/*z* for **OE** fail to appear in the corresponding Mass spectrum, which may be attributed to highly reactive and vulnerable characteristic of epoxy group.

The ORTEP plot of **OA** is shown in Fig. 3 and its crystal data in Table 1. Based on XRD single crystal diffraction analysis, **OA** is a triclinic system with characteristic bond lengths and angles similar to those reported by Martinova et al. [22]. The purified product of **OE** via recrystallization was found out to be polycrystalline, which was evidenced in powder X-ray diffraction characterization, giving several sharp peaks at $2\theta=20$, 23, 25° etc. The difficulty of obtaining single crystal of **OE** might be due to the presence of epoxy group to render the products highly soluble in

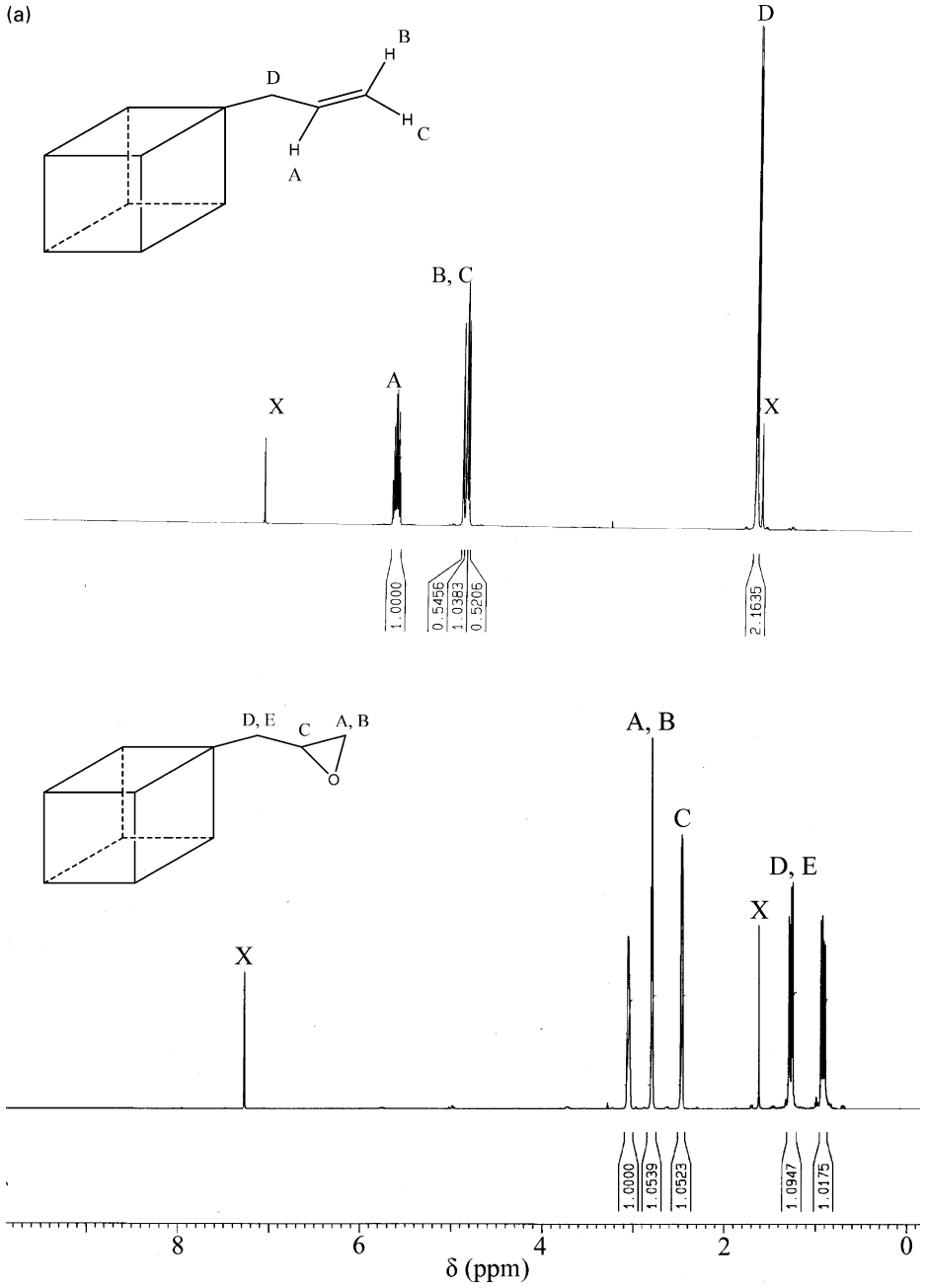

Fig. 2. (a) ^{1}H NMR spectra of **OA** and **OE** in $CDCl_3$ (symbol X in the spectra). (b) ^{13}C NMR of **OA** and **OE** (symbol X in the spectra).

common solvents. Thus, it is difficult to find a suitable solvent for recrystallization.

Fig. 4 shows the DSC curves of **OA** and **OE** under nitrogen atmosphere. For the case of **OA**, a large endothermic peak centered at 71 °C during heating is assigned to melting of **OA** crystal. As cooling from 120 °C to room temperature, an exothermic peak at 65 °C due to the recrystallization peak is observed. Heat of melting of **OA** is estimated to be 36.5 J/g. When **OE** is heated to 120 °C, two endothermic peaks appear at 51 and 58 °C, which is another evidence of polycrystallinity besides the XRD result described above. A small recrystallization peak appears at 46 °C during the cooling cycle of **OE**. Hence, it is concluded that the packing of **OE** is less efficient than that of **OA**. The presence of epoxy on POSS is likely to introduce more than one way of packing from the comparison of **OA** and **OE**. The thermal decomposition temperature (T_d, estimated from 5% loss of initial weight) of **OA** and **OE** are observed at 190 and 252 °C, respectively. Thermally-induced ring opening and polymerization might contribute to the higher thermal stability of **OE** than that of **OA**. The percentages of experimental residue at 900 °C are 52.1 and 54.9% for **OA** and **OE**, respectively, while the theoretical residue percentage 55.9 and 52.5%. Note that the theoretical values are

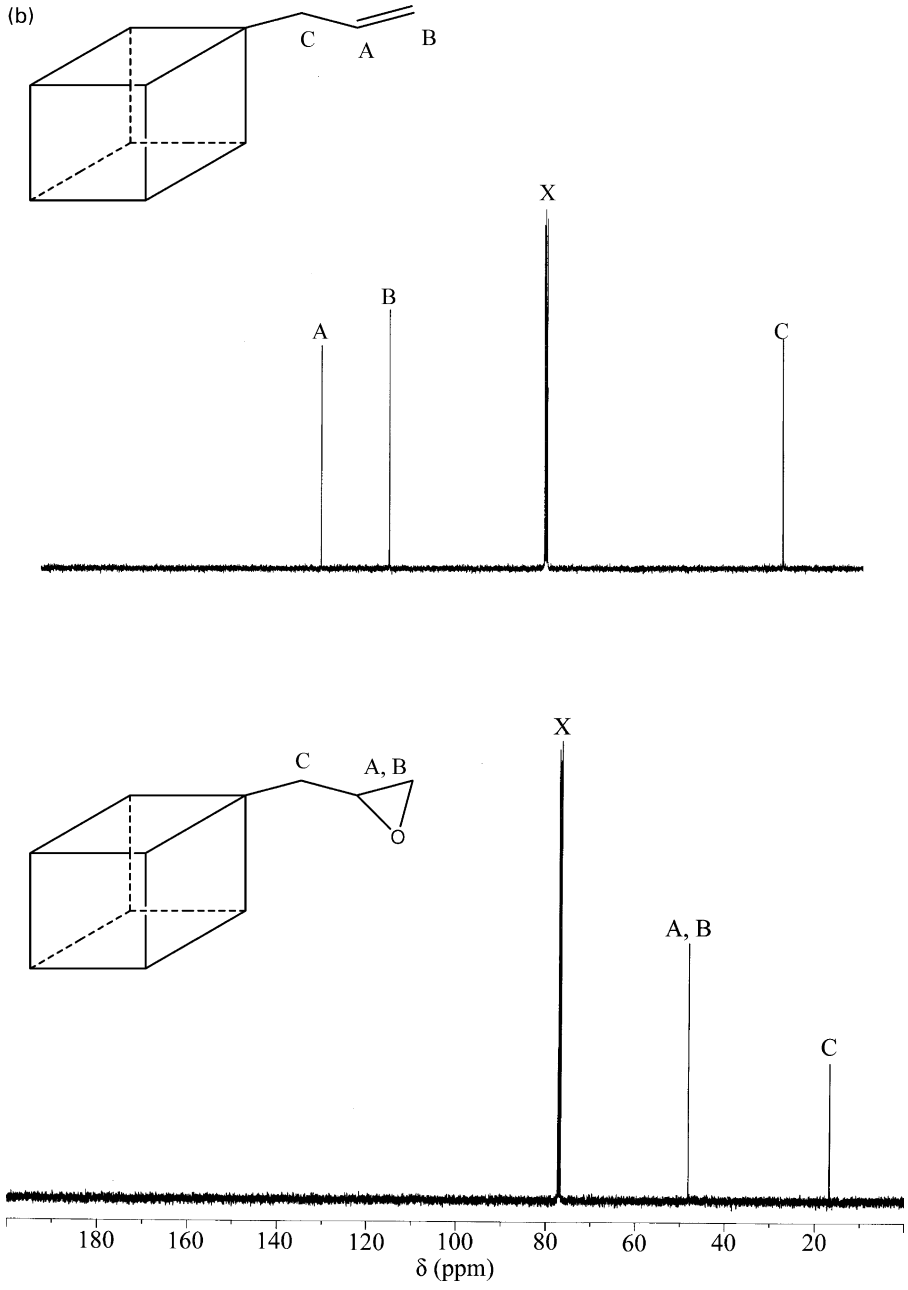

Fig. 2 (*continued*)

based on the assumption that all peripheral organic arms attaching to cage decomposed completely while the cages remain due to low volatility. The lower experimental value than the theoretical for **OA** could be resulted by formation of some volatile silicon-containing species [8]. However, formation of network structure due to thermally-induced epoxide ring opening polymerization might result in retardation on escape of volatile species thus higher T_d was obtained for the case of **OE**. Note that a large exothermic peak around 130 °C in the DSC thermogram of **OE** and the large reduction of the epoxy IR peak suggests the ring-opening reaction of **OE**.

*3.2. Preparation and characterization of **OE-DDM** hybrid nanocomposites*

The IR spectra of **OE** and **OE-DDM** hybrids are shown in Fig. 5. The peak at 1325 cm^{-1} increases in intensity with increasing DDM content as shown in the figure. This peak is absent in pure DDM, as well as in tertiary amine containing one aromatic and two aliphatic substituents but present in secondary amine containing exactly one aromatic and one aliphatic substituent. For example, both methylphenylamine and ethylphenylamine absorb at 1322 cm^{-1}, whereas dimethylphenylamine absorbs at 1349 and 1229 cm^{-1}.

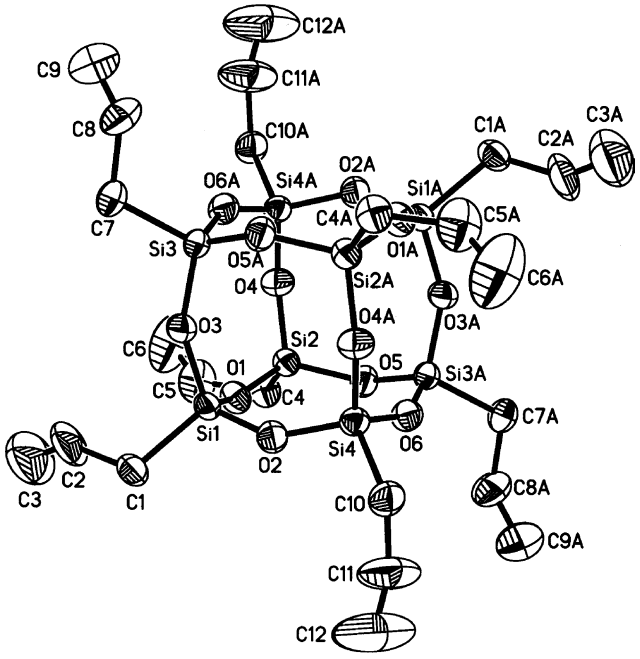

Fig. 3. ORTEP plots of **OA**.

Hence, it suggests that the peak at 1325 cm^{-1} represents a secondary amine. It also indicates that the four N–H bonds on DDM do not react completely during curing. Since the epoxide lying closed to the bulky phenyl group of the diamine and the gigantic silsesquioxane cage, the second N–H group on the amino probably hardly reacts with another epoxide.

Compared with **OE**, the 1110 cm^{-1} peak of hybrids is observed to broaden in IR spectra. The phenomenon is believed to be resulted from aromatic C–H in-plane bending due to presence of DDM rather than destruction of silsesquioxane cage. The solid state CP/MAS ^{29}Si NMR will give further support on the retention of the silsesquioxane cage later. The peak at 837 cm^{-1} is characteristic of

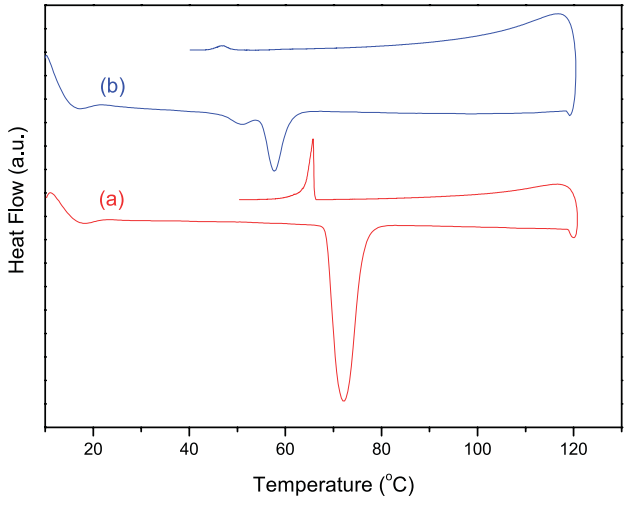

Fig. 4. DSC thermograms of (a) **OA** and (b) **OE** at a heating rate of 20 °C/min.

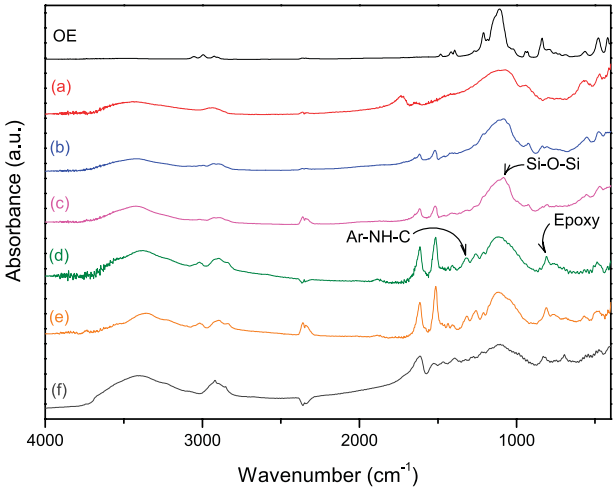

Fig. 5. FTIR absorption spectra of **OE** (uncured), and the hybrid materials (a): **OE-DDM-0**, (b): **OE-DDM-50**, (c): **OE-DDM-100**, (d): **OE-DDM-200**, (e): **OE-DDM-300**, and (f): **OE-FPA-200**.

epoxy group, which decreases rapidly in intensity with increasing DDM content due to a ring opening reaction. The peak at 3425 cm^{-1} for **OE-DDM-50** is observed to shift to a lower wavenumber as the DDM content increases: 3387 cm^{-1} for **OE-DDM-200** and 3361 cm^{-1} for **OE-DDM-300**. It is attributed to extensive and increasing amount of hydrogen bonding within the hybrid materials. The IR spectrum of **OE-FPA-200** is also shown in Fig. 5. The broad peak at 3405 cm^{-1} indicates the prevalence of O–H and N–H bonds, which implies successful reaction between diamine and epoxy-containing silsesquioxane, as well as extensive hydrogen bonding.

The number of remaining epoxy groups is a direct indication of extent of reaction between **OE** and DDM, which can be approximately estimated by IR curve fitting. Fig. 6 shows the average number of residual epoxy groups per cage with the DDM content in the hybrid materials. The line A is based on the conventional concept that every N–H group reacts with exactly one epoxy group, regardless of steric hindrance. The line B is based on the hypothesis by Laine et al., which suggested only one of two N–H bonds an amine group reacted with epoxy [8,9]. The remaining N–H becomes inactive due to the highly congested environment. The line C is the results of IR curve fitting in the present study. The average number of epoxy groups left per cage in line C is 6.19, 4.42, 2.64, and 0.3 for DDM of 50, 100, 200 and 300% of stoichiometric ratio, respectively. The average percent of reacted N–H bond in diamines was recalculated to be only 45.2, 44.7, 33.5 and 32.1% for **OE-DDM-50**, **OE-DDM-100**, **OE-DDM-200** and **OE-DDM-300**, respectively. Although, the average number of residual epoxy groups decreases with increasing DDM content, it deviates slightly from the line B and substantially from the line A. The deviation from the Lines A and B probably originates from the gradually-built steric hindrance during the curing process, in which a primary amine may not react at all due to

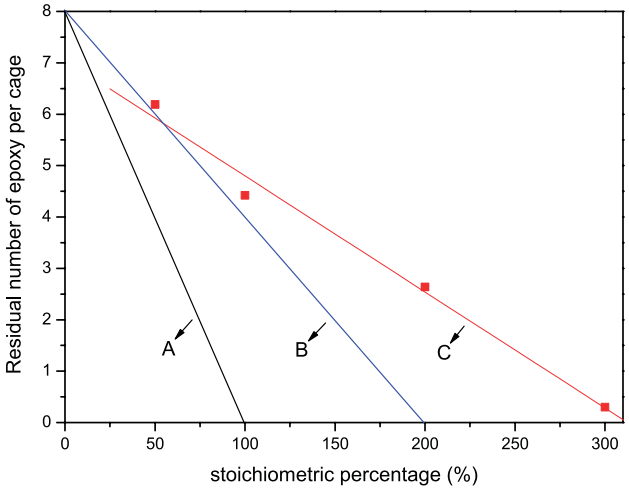

Fig. 6. Variation of epoxy residue group per cage with stiochiometric ratio of amine group to epoxy group: line A: complete consumption of N–H bond on amino group by epoxide; line B: exactly one of the two N–H groups reacted with epoxide, line C: results of IR curve fitting of **OE-DDM** hybrid materials.

absence of adjacent epoxy groups or low tendency toward reaction due to overly congested surroundings. For the case of **OE-FPA-200**, it is not possible to estimate the average number of epoxy group reacted via curve fitting due to the overlap of the peak at 838 cm^{-1}.

One of the major concerns about POSS-related materials is that if the cage-structured silsesquioxanes remain intact during synthesis, especially at higher reaction temperatures. Fig. 7(a)–(c) shows the ^{29}Si CP/MAS NMR results of **OE**, **OE-DDM-200**, and **OE-FPA-200**, with peaks located in −69.76, −68.56 and −67.46 ppm, respectively. The similar peak near −70 ppm suggests that the retention of the cage structure. Besides, if the cage was destroyed during preparing hybrid materials, a characteristic peak of SiF_6^{2-} would be observed −191 ppm [23] in Fig. 7(c). However, the small peak around −100 ppm in Fig. 7(c) might imply the presence of silicon-containing species with coordination number of five [23], and silicon-fluorine interaction may also contribute, as suggested in the literature [24–28]. In ^{19}F CP/MAS NMR of **OE-FPA-200**, several peaks, such as the ones at −80, −105, −124 and −170 ppm, appeared in addition to the one at −61 ppm, which originated from FPA monomer. Therefore, there must be several different immediate surroundings to fluorine species. Based on the results of ^{19}F and ^{29}Si CP/MAS NMR, it was hypothesized that some of the silicon became penta-coordinated during preparation, and could have various degree of silicon–fluorine interaction depending on mutual distance and orientation. The unexpected interaction between silicon and fluorine atoms could further reduce segmental mobility in the highly crosslinked **OE-FPA-200** and contribute to its thermal and mechanical properties.

Fig. 8 demonstrates the TGA thermograms of **OE-DDM** and **OE-FPA** hybrids. All hybrid materials, have T_d around

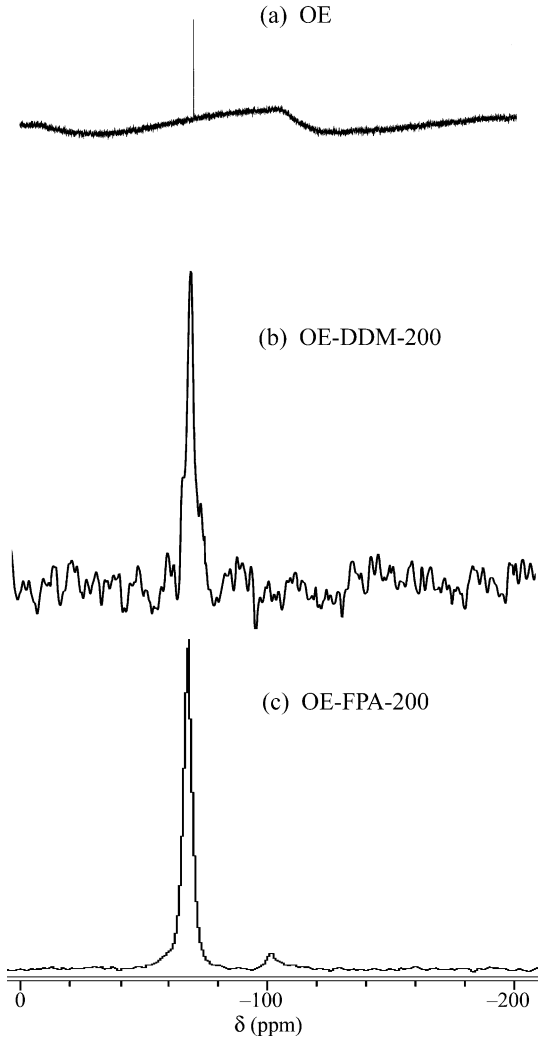

Fig. 7. ^{29}Si CP/MAS NMR spectra of (a) **OE**, (b) **OE-DDM-200**, and (c) **OE-FPA-200**.

270 °C except **OE-FPA-200** with 286 °C and **OE-DDM-300** with 257 °C, which is slightly higher than that of **OE** with 252 °C. Since formation of crosslinked structure is believed to contribute to a higher thermal stability, the lower T_d of **OE-DDM-300** may be attributed to the higher percentage of unreacted amino groups. Experimental char yields for all hybrid materials, as listed in Table 2, are higher than theoretical values. It might be because the volatile species is trapped in the highly crosslinked structure [29,30] or the characteristic of high char yield on POSS or silicon-containing epoxy nanocomposites [8,9]. The T_d (<300 °C) of the **OE**/diamines hybrid materials is lower than those OG/DDM and OC/DDM with T_d exceed 350 °C reported in the literature [9]. It might be due to the substituents on the cage: the siloxane side arms have higher thermal degradation stability than the direct linkage of aliphatic ones [1]. Cleavage of Si–C or C–C bonds or the residual 2,3-epoxypropyl and DDM moiety might result in a lower thermal decomposition temperature of the prepared hybrid materials.

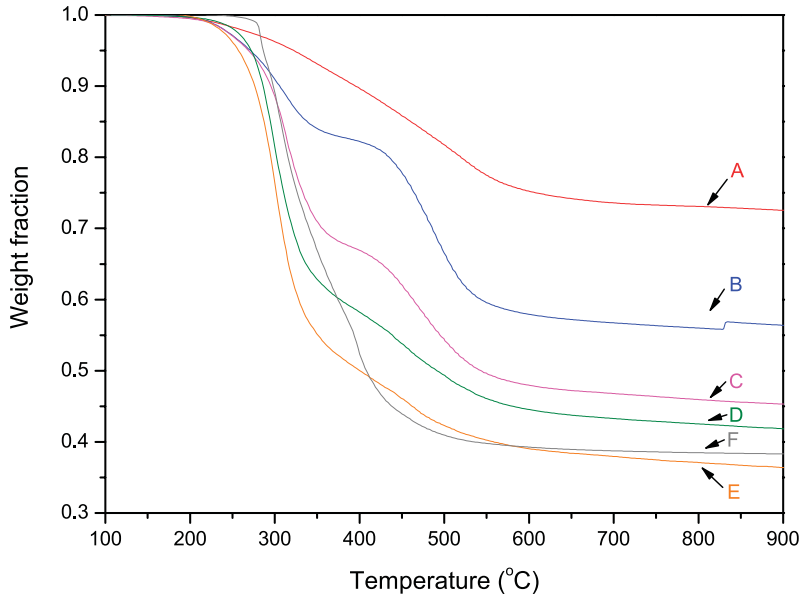

Fig. 8. TGA thermograms of (a) **OE-DDM-0**, (b)**OE-DDM-50**, (c) **OE-DDM-100**, (d) **OE-DDM-200**, (e) **OE-DDM-300** and (f) **OE-FPA-200**.

The DSC thermograms of **OE-DDM** and **OE-FPA-200** hybrids show no apparent glass transition temperature (T_g). It indicates that shortening the distance between cage and epoxy group may increase T_g. Fig. 9 shows the TMA curves of **OE-DDM-200–300** and **OE-FPA-200**. **OE-DDM-50** and **OE-DDM-100** were excluded from TMA analysis due to their brittle nature and inability of forming suitable bulk materials. Different slopes on TMA curves of **OE-DDM-200**, **OE-DDM-300**, and **OE-FPA-200** are observed in the figure. The T_g determined from the TMA curves are 120, 110, and 165 °C for **OE-DDM-200**, **OE-DDM-300**, and **OE-FPA-200**, respectively. The coefficients of thermal expansion (CTE) of the hybrids, **OE-DDM-200**, **OE-DDM-300**, and **OE-FPA-200**, are 98, 114 and 86 μm/m °C, respectively, as listed in Table 2. The CTEs of the hybrid materials are 20–30% lower than that of poly(tetrafluoroethylene) (150 μm/m °C, in the range 25–200 °C). The extensive crosslinking and hydrogen bonding are thought to be the major factors contributing to the dimensional stability of the hybrids, which are further explained in the next section.

The thermal–mechanical properties of the prepared hybrid materials are further studies by DMA, as shown by Fig. 10. The storage modulus for **OE-DDM-200**, **OE-DDM-300**, and **OE-FPA-200** at 30 °C are 1.8, 0.45 and 1.8 GPa, respectively. Except for **OE-DDM-300**, the values

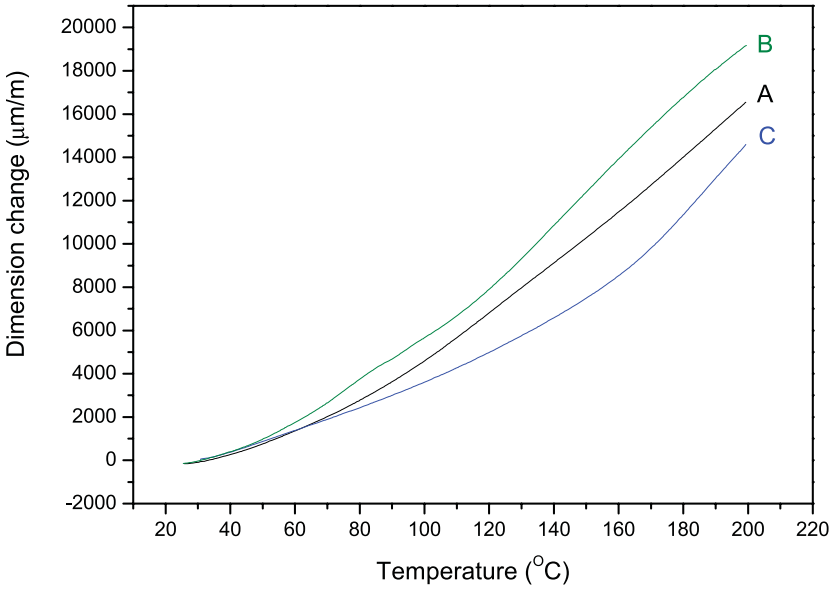

Fig. 9. TMA curves of (a) **OE-DDM-200**, (b) **OE-DDM-300**, and (c) **OE-FPA-200**.

Table 2
Properties of **OE-DDM-200**, **OE-DDM-300** and **OE-FPA-200**

Hybrid	T_d (°C)	Theo. char (%)[a]	Expt. char (%)	T_g (°C)[b]	Storage modulus (30 °C, GPa)	Storage modulus (250 °C, GPa)	CTE[c] (μm/m °C)	Dielectric constant[d]	Loss factor
OE-DDM-200	272	24.6	41.8	120	1.8	0.17	98	2.93	0.05670
OE-DDM-300	257	19.8	36.3	115	0.45	0.04	114	N/A	N/A
OE-FPA-200	286	26.3	38.2	170	1.8	0.3	86	2.19	0.03626

[a] Theoretical char yields were estimated based on the assumption that inorganic fraction of **OE**.
[b] Determined from DMA
[c] Determined from TMA.
[d] Determined at 100 kHz.

are of the same order of magnitude as those reported by Laine and his coworkers [8,9]. When heated to 250 °C, **OE-DDM-200**, **OE-DDM-300**, and **OE-FPA-200** have respective storage modulus of 0.17, 0.04 and 0.3 GPa, which are significantly higher than those of **OC/DDM** or **OG/DDM** hybrid materials [8,9]. Storage modulus of **OE-FPA-200** is similar to that of **OE-DDM-200** at 30 °C, but is almost twice at 250 °C. **OE-DDM-300** has a lower storage modulus than **OE-DDM-200**, which is attributed to the excessive content of diamine in the hybrid material. In **OE-DDM-300**, a significant proportion of diamine is singly-bonded to silsesquioxane cages. The loose ends of singly-bonded diamines rotate more freely and demand more free volume, thereby acting as lubricant and weakening the strength of crosslinking structure. The tanδ peaks occurred at 120, 115 and 170 °C for **OE-DDM-200**, **OE-DDM-300**, and **OE-FPA-200**, respectively, which are also higher than **OC/DDM** or **OG/DDM** hybrid materials with 60–100 °C [8,9]. To our surprise, **OE-FPA-200** had its tanδ peak as high as 170 °C, which is even higher than widely applied stoichiometric **DGEBA/DDM** material (160 °C). The tanδ peak of the **OE-FPA-200** is small and broad, confirming the limited scale of thermal relaxation. In **OE-FPA-200**, the intercage distance is smaller since FPA consists of only one aromatic ring, instead of two in DDM. The difference in rigidity of FPA and DDM lies in that the latter bears a flexible methylene between its two aromatic rings, which causes the molecule and **OE-DDM** hybrids to undergo thermally induced motions more easily. FPA also acts as a pseudo-multifunctional agent and probably undergoes more extensive crosslinking reaction via silicon–fluorine interaction attributed to donation and acceptance of electron density between the two atoms [24–28] and additional hydrogen bonding between residual hydroxy groups and fluorine atoms. The heavily and covalently crosslinked structure and prevalent hydrogen bonding contribute to the limited scale of thermal relaxation process.

The dielectric constants and loss factors factors of **OE-DDM-200**, **OE-DDM-300** and **OE-FPA-200** hybrid materials are shown in Table 2. The dielectric constants of **OE-DDM-200** and **OE-FPA-200** are 2.93 and 2.19, respectively. The presence of fluorine atom in **OE-FPA-200** reduces the dielectric constant significantly, due to the high electronic affinity of fluorine atom. The power factor is lower for **OE-FPA-200** as well, which means that the material absorbs less energy under the same condition. The tendency to align polarizable groups such as N–H and O–H with applied alternating electrical field determined the dielectric properties in a sense that the more easily these groups align with the field, the higher the dielectric constant and the more energy they store. The extensively connected nature of **OE-FPA** hybrid material, due to covalent bonding between cages in shorter distance, hydrogen bonding between intercage tethers and silicon–fluorine interaction, rendered alignment more difficult compared to that of **OE-DDM**. With superior performance in thermal and

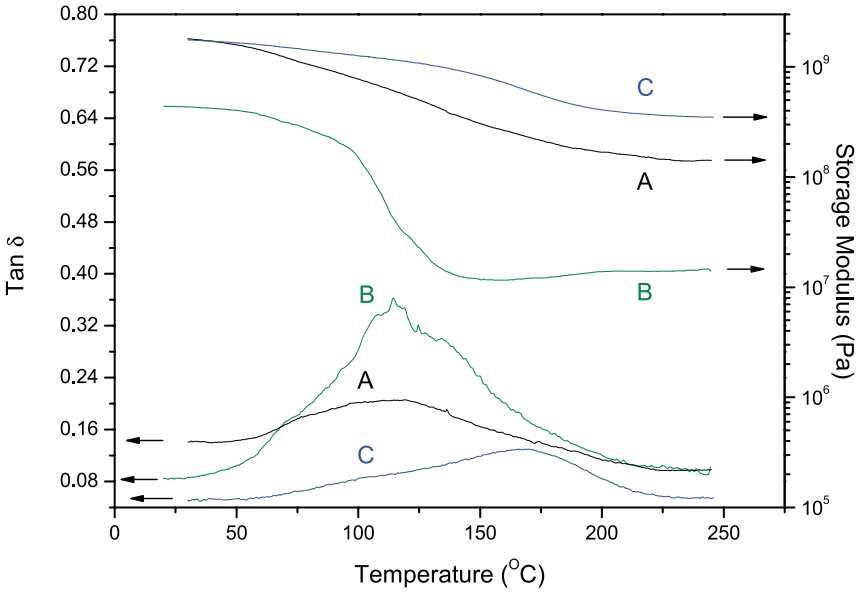

Fig. 10. Storage modulus and tan δ curves of (a) **OE-DDM-200**, (b) **OE-DDM-300** and (c) **OE-FPA-200**.

mechanical properties, low CTE and dielectric constant, **OE-FPA-200** has the potential applications as electronic packaging materials.

4. Conclusions

Hybrid materials from a new polyhedral oligomeric silsesqioxane, octa(2,3-epoxypropyl)silsesquioxane (**OE**)/diamines were prepared and characterized. The successful synthesis of **OA** and **OE** were demonstrated by FTIR, ^{1}H, ^{13}C, ^{29}Si NMR, and XRD. The FTIR studies suggested that the N–H bond in diamines was not completely reacted with epoxy group due to steric hindrance and also extensive hydrogen bonding existed in the hybrid materials. The retention of the cage structure in the prepared hybrid materials was suggested by the FTIR and ^{29}Si NMR studies. The **OE/FPA** hybrid materials had superior thermal/mechanical characteristics than the **OE/DDM** due to the higher rigidity of the FPA than that of DDM or the silicon-fluorine interaction enhancing crosslinking reaction or hydrogen bonding. The excellent physical properties of the prepared **OE/FPA** may have potential applications as high performance materials.

Acknowledgements

We would like to thank Mr Hung-Wen Su of AGI Corporation for his assistance on DMA measurement, Professor Wen-Bin Liau and Mr Ling-Yueh Yang, of Department of Materials Science and Engineering, National Taiwan University for measuring the dielectric constants of the prepared hybrid materials. Financial support of this work from National Science Council of Taiwan and Ministry of Economic Affairs are also appreciated.

References

[1] Banley RH, Itoh M, Sakakibara A, Suzuki T. Chem Rev 1995;95:1409.
[2] Lee JK, Char K, Rhee HW, Ro HW, Yoo DY, Yoon DY. Polymer 2001;42:9085.
[3] Yang CC, Chen WC. J Mater Chem 2002;12:1138.
[4] Chen WC, Lee LH, Chen BF, Yen CT. J Mater Chem 2002;12:3644.
[5] Lee LH, Chen WC, Liu WC. J Polym Sci, Polym Chem 2002;40:1560.
[6] Sheng YJ, Lin WJ, Chen WC. J Chem Phys 2004;15:9693.
[7] Lichtenhan JD, Otonari YA, Carr MJ. Macromolecules 1995;28:8435.
[8] Choi J, Harcup J, Yee AF. J Am Chem Soc 2001;123:11420.
[9] Choi J, Yee AF, Laine RM. Macromolecules 2003;36:5666.
[10] Lee A, Lichtenhan JD. Macromolecules 1998;31:4970.
[11] Kim GM, Qin H, Fang X, Sun FC, Mather PT. J Polym Sci, Polym Phys 2003;41:3299.
[12] Abad MJ, Barral L, Fasce D, Williams RJJ. Macromolecules 2003;36:3128.
[13] Chen WC, Wang YZ, Kuo SW, Huang CF, Tung PT, Chang FC. Polymer 2004;45:6897.
[14] Tamaki R, Tanaka Y, Asuncion MZ, Choi J, Laine RM. J Am Chem Soc 2001;123:12416.
[15] Leu CM, Chang YT, Wei KH. Macromolecules 2003;36:9122.
[16] Zhang C, Babonneau F, Bonhomme C, Laine RM, Soles CL, Hristov HA, et al. J Am Chem Soc 1998;120:8380.
[17] Neumann D, Fisher M, Tran L, Matisons JG. J Am Chem Soc 2002;124:13998.
[18] Kim KM, Keum DK, Chujo Y. Macromolecules 2003;36:867.
[19] Lin WJ, Chen WC, Wu WC, Niu YH, Jen AKY. Macromolecules 2004;37:2335.
[20] Constable GS, Lesser AJ, Coughlin EB. Macromolecules 2004;37:1276.
[21] Zhang C, Laine RM. J Organomet Chem 1996;521:199.
[22] Martynova TN, Korchkov NP, Semyannikov PP. J Organomet Chem 1983;258:277.

[23] Marsmann HC. Encyclopedia of nuclear magnetic resonance. vol. 7. New York: Wiley; 1996, p. 4386.
[24] Kumara Swamy KC, Chandersekhar V, Harland JJ, Holmes JM, Day RO, Holmes RR. J Am Chem Soc 1990;112:2341.
[25] Huang XH, He PY, Shi GQ. J Org Chem 2000;65:627.
[26] Bassindale AR, Pourny M, Taylor PG, Hursthouse MB, Light ME. Angew Chem, Int Ed 2003;42:3488.
[27] Saxena A, Fujiki M, Naito M, Okoshi K, Kwak G. Macromolecules 2004;37:5873.
[28] Iwamiya JH, Maciel GE. J Am Chem Soc 1993;115:6835.
[29] Lee LH, Chen WC. Chem Mater 2001;13:1137.
[30] Yu YY, Chen CY, Chen WC. Polymer 2003;44:593.